Available online at www.sciencedirect.com
ScienceDirect
Advances in Space Research 40 (2007) 719–733
ADVANCES IN SPACE RESEARCH (a COSPAR publication)
www.elsevier.com/locate/asr

Gravity-wave breaking: Linear and primary nonlinear dynamics

Ulrich Achatz *

Leibniz-Institut für Atmosphärenphysik an der Universität Rostock, Schloßstr. 6, 18225 Kühlungsborn, Germany

Received 28 November 2006; received in revised form 23 March 2007; accepted 29 March 2007

Abstract

In a summary of recent work on the breaking of gravity waves (GWs) and the corresponding onset of turbulence the question of critical thresholds is given a systematic discussion. Contrary to a widespread belief static and dynamic stability do not indicate a GW's stability against breaking. Low-frequency inertia–gravity waves can be destabilized by singular vectors even if their amplitude is too weak to produce local Richardson numbers less than a quarter. High-frequency gravity waves have horizontal gradients strong enough so that even at statically and dynamically stable amplitudes they are destabilized by normal modes. The dynamics of the processes is discussed within a framework which takes a careful path from linear stability analyses to direct numerical simulations. The latter show that subcritical GW breaking can lead to turbulence of a strength as observed in the middle atmosphere. In many cases the GW amplitude is reduced way below the conventional thresholds of static or dynamic instability.

Keywords: Gravity waves; Instabilities; Normal modes; Singular vectors; Optimal perturbations; Turbulence; Middle atmosphere

1. Introduction

Gravity waves (GWs) are thought to be a key element in the generation of oceanic turbulence which again seems to be vital for keeping the thermohaline circulation in motion (Müller et al., 1986; Staquet and Sommeria, 2002; Wunsch and Ferrari, 2004). Moreover, their relevance for an understanding of the general circulation in the middle atmosphere has been established for quite a while (Hines, 1960; Houghton, 1978; Lindzen, 1981; Holton, 1982, 1983; Garcia and Solomon, 1985). Due to various processes GWs are radiated from the troposphere and stratosphere. In the course of their upward propagation they are amplified since energy is conserved in an ambient medium with decreasing density. At some stage they are too strong to sustain themselves and begin depositing momentum, thus driving the global circulation in the mesosphere. Although there is a general agreement on this overall picture many uncertainties remain. These are well documented, e.g. by a considerable number of schemes available for the parameterization of GWs in general circulation models (Lindzen, 1981; Medvedev and Klaassen, 1995; Hines, 1997a,b; Alexander and Dunkerton, 1999; Warner and McIntyre, 2001). They differ in the basic picture of GW dynamics in the middle atmosphere, and no consensus has been found yet on which of them is the correct one. Even worse, each scheme offers a nonnegligible set of free parameters which are today mainly used as tuning parameters.

One among the numerous causes for this situation is that there are still open questions concerning the conditions under which a GW will begin depositing its momentum in the ambient larger-scale flow, and how this wave breaking proceeds (Fritts and Alexander, 2003). Moreover, the knowledge which has already been gathered has not completely found its way into any up-to-date parameterization, partly due to the seemingly too complex picture drawn by respective studies. This is indeed a very hard problem, but at least in respect to the interpretation of observations we might make more immediate use of the latest findings. Often one still sees turbulence onset in the atmosphere being discussed in terms of a wave crossing

* Tel.: +49 38293 68340; fax: +49 38293 6850.
E-mail address: achatz@iap-kborn.de.

0273-1177/$30
doi:10.1016/j.asr.2007.03.078

the threshold of static instability, corresponding to an overturning of contours of potential density or potential temperature, or dynamic instability, where the local vertical gradient of the horizontal wind causes the local Richardson number to fall below 1/4. In fact, these are misleading concepts in the context of wave breaking. They neglect the impact of horizontal gradients in the wave, and they also do not take the possibility of nonmodal instabilities into account. It is important for the observational community to recognize this so as to avoid misinterpretations of their data. On this background the purpose of this review is twofold: (1) It summarizes the most important aspects of our knowledge under which conditions a GW will start breaking, and (2) it gives a summary of recent respective work of the author which hopefully might also help getting a clearer conceptual picture of GW breaking itself (Achatz, 2005; Achatz and Schmitz, 2006a,b; Achatz, 2007a,b). The central paradigm of wave-turbulence interaction addressed in this work is the breaking of a single wave, leaving aside the dynamics of a whole spectrum of GWs. In this context a major theme is to carefully take the path from linear stability analyzes to direct numerical simulations (DNS) of GW breaking. By first identifying the dynamically most relevant perturbations and then distinctly perturbing the GW by these in a DNS one can improve our understanding of typical features of the breaking process. This knowledge is to be used as complementary information to the one gained already from three-dimensional (3D) DNS where the GW is perturbed by random noise (Fritts et al., 2003, 2006).

With this purpose the article is structured as follows: Section 2 discusses some general aspects of the linear dynamics of GW breaking. Section 3 summarizes the linear dynamics of inertia–gravity-wave breaking, with a special focus on singular vectors (SVs), and the primary nonlinear dynamics developing after perturbing the IGW by its leading normal modes or SVs. An analogous discussion of the dynamics of high-frequency gravity-wave breaking can be found in Section 4. Section 5 gives a short synthesis and discussion. Due to the author's background the focus is more on the atmosphere than on the ocean, but the discussed dynamics is certainly also part of oceanic GW dynamics.

2. General aspects of the linear dynamics of GW breaking

The analyzed situation is sketched in Fig. 1. A GW exhibits phase propagation at an inclination angle Θ with respect to the horizontal. Note that due to the dispersiveness of GWs the phase propagation actually points downward while the group velocity is directed upward. The following considerations assume that all interesting processes happen within an altitude range of the order or less than an atmospheric scale height so that the Boussinesq approximation can be used. The coordinate system moves with the ambient flow (assumed to be constant), so that within this framework the wave frequency is given by

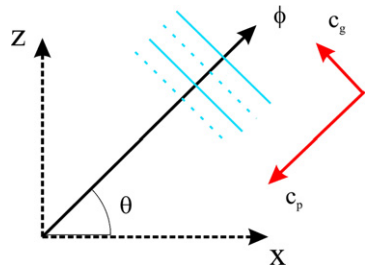

Fig. 1. Sketch of a GW exhibiting a phase propagation at an inclination angle Θ with respect to the horizontal, indicated by the x-axis. Lines of constant GW phase are indicated in blue. The group velocity $\mathbf{c}_g$ is directed upward, while the phase velocity $\mathbf{c}_p$ points downward. (For interpretation of the references to colour in this figure legend, the reader is referred to the web version of this article.)

$$\omega = \pm\sqrt{f^2 \sin^2\Theta + N^2\cos^2\Theta}. \tag{1}$$

Here f is the local Coriolis parameter, and N the Brunt–Vaisala frequency. At positive vertical wavenumber the positive (negative) branch has upward (downward) phase propagation, so that in the atmospheric context the latter is the more interesting one. GWs are influenced both by the earth's rotation and by the stratification of the ambient medium. According to the respective relevance of these factors GWs can be subdivided into two classes. At steep phase propagation ($|\tan\Theta| > N/f$) rotation is relevant, and the approximate dispersion relation is $\omega \approx \pm f[1 + (N^2/f^2)\cot^2\Theta]$. These long-period waves are known as *inertia–gravity waves* (IGWs). An important property of them is that their horizontal velocity field has an elliptic polarization which becomes increasingly circular as $\Theta \to \pm\pi/2$. The other class, here called *high-frequency gravity waves* (HGWs), has less steep phase propagation ($|\tan\Theta| < N/f$), so that $\omega \approx \pm N\cos\Theta$. These have a linearly polarized velocity field which lies in the x–z-plane of wave propagation. Note that usually $N \gg f$ so that the range of inclination angles for IGWs is very small.

The linear stability analysis asks about the fate of any infinitesimally small perturbation of a GW. This question can be posed in various ways. In one variant one determines the normal modes (NMs) of the problem. As sketched in Fig. 2 these have, within the limits of linear theory where all nonlinear interactions potentially leading to a turbulent cascade are neglected, a rather simple time dependence of their amplitude or energy. It is strictly exponential. A NM either decays exponentially, has constant amplitude, or it grows exponentially. A NM analysis determines at least the leading NMs, i.e. with the largest growth rate. If any NM with positive growth rate is found, the result of the analysis is an instability of the basic gravity wave. In the opposite case the diagnosis is that the wave can continue propagating without any interaction with the ambient flow, neglecting the effects of viscosity and diffusion. A limitation of NM analyses is that they can only be done for a basic state which is time independent. As seen below, this is no problem for a monochromatic GW.

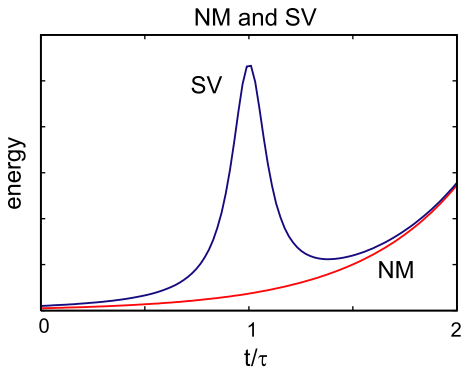

Fig. 2. Sketch of the time dependence of the energy of a normal mode (NM) or a singular vector (SV) within linear theory. The optimization time for the SV is $t = \tau$.

One should also be aware that the well-known conventional instability thresholds have been derived from just such analyses, assuming a basic state without wave, but a purely vertically dependent stratification and horizontal velocity field. Under such conditions one can show easily the existence of growing NMs if there is a *static instability* so that at least at one altitude the total static stability becomes negative, i.e.

$$N_{\mathrm{tot}}^2 = N^2 + \frac{\mathrm{d}b}{\mathrm{d}z} < 0. \tag{2}$$

Here $b(z) = g(\theta - \overline{\theta})/\theta_0$ is the buoyancy, to be determined from the deviation of the potential temperature θ from a reference profile $\overline{\theta}$. The latter also determines the Brunt–Vaisala frequency via $N^2 = (g/\theta_0)\mathrm{d}\overline{\theta}/\mathrm{d}z$, with θ_0 being a constant representative value, while g is the gravitational acceleration. Oceanographers would rather define buoyancy and N^2 via (potential) density profiles, i.e. $b = (g/\rho_0)(\overline{\rho} - \rho)$ and $N^2 = -(g/\rho_0)\mathrm{d}\overline{\rho}/\mathrm{d}z$. Since static instability is a very important concept it is often used to define the GW amplitude a. If $a > 1$ there is a least one phase in the GW where $N_{\mathrm{tot}}^2 < 0$, with the buoyancy field taken from the GW. Taking also the horizontal velocity field into account, it was shown by Howard (1961) and Miles (1961) that, if there is a growing NM, then at least at one altitude the local Richardson number is less than a quarter, i.e.

$$Ri = \frac{N_{\mathrm{tot}}^2}{(\mathrm{d}u/\mathrm{d}z)^2 + (\mathrm{d}v/\mathrm{d}z)^2} < \frac{1}{4}. \tag{3}$$

Here u and v are the basic state horizontal velocity components in x- and y-direction, in the present context given by the corresponding GW fields. This is the condition for *dynamic instability*. It is a necessary condition for instability, not a sufficient one. Note that both of the two instability concepts have been derived under the assumption that either u, v, or b have any horizontal gradients! This is most problematic in an application of these concepts to the instability of a HGW, which does have considerable horizontal gradients in all its dynamical fields. Indeed, as will be discussed below, HGWs turn out to be unstable at amplitudes way below any of the two thresholds.

An alternative concept to normal modes is that of optimal growth of singular vectors (SVs). Given a predefined optimization time τ the corresponding leading singular vector maximizes the ratio $E(\tau)/E(0)$ between the perturbation energy at this time and its initial value (Boberg and Brosa, 1988; Farrell, 1988a,b; Trefethen et al., 1993). As shown in Fig. 2, typically the energy of an SV, once again within linear theory, exhibits quite rapid growth between $t = 0$ and $t = \tau$, then decays again, and finally approaches asymptotically the time dependence of the leading NM. Two interesting things can happen: (1) It is conceivable that the leading SV grows so strongly that it can initiate an irreversible nonlinear development before the more slowly growing NM has had time to do so. This might be relevant at sufficiently strong initial perturbation amplitudes. (2) Even more interesting is that SVs can grow even when there is no growing NM at all. Thus, in situations where a NM analysis would diagnose stability of a GW, a SV analysis can help us understanding situations where turbulence onset is observed in spite of the NM stability. As will be shown below this can be relevant for the breaking of IGWs. For a more thorough discussion of NMs and SVs, and the difference between the two one could also consult Farrell and Ioannou (1993b,a), Achatz (2005), and Achatz and Schmitz (2006a,b).

In the specific situation to be analyzed here the calculations can be simplified by a useful coordinate transformation (see Fig. 3). One rotates the x- and z-axis about the y-axis by $\Theta - \pi/2$, so that the new, slanted, vertical axis is parallel to the direction of phase propagation of the GW. The coordinate system is then also moved downward by the GW's phase velocity, so that the new reference system is described by the coordinates ξ along the rotated x-axis, y, and the wave phase ϕ. Within this reference system the GW is time independent. This enables a classic NM

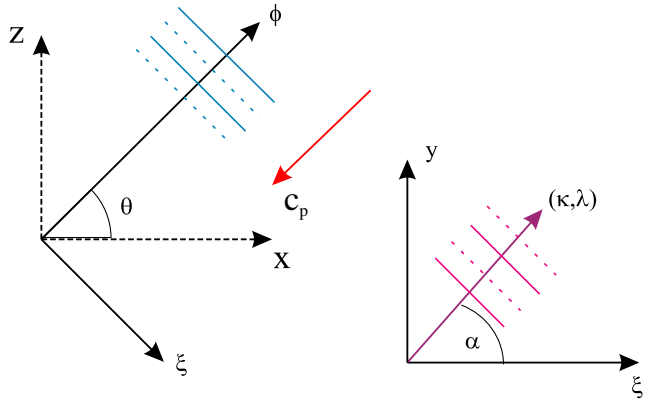

Fig. 3. Sketch of the transformed coordinate system used for the linear stability analysis of a GW (phase lines in blue). The perturbation (purple) is a monochromatic wave in the plane spanned by the ξ-axis, i.e. the rotated x-axis, and the y-axis. (For interpretation of the references to colour in this figure legend, the reader is referred to the web version of this article.)

analysis. It also only depends on one spatial coordinate, the GW phase. The symmetry of this basic state with respect to the slanted horizontal coordinates ξ and y has the immediate consequence that both the NMs and the SVs are monochromatic waves in the slanted horizontal plane, i.e. their velocity field $\mathbf{v}'$ and buoyancy b' can be written as

$$(\mathbf{v}', b')(\mathbf{x}, t) = \Re\left[(\widehat{\mathbf{v}}, \widehat{b})(\phi, t)\mathrm{e}^{\mathrm{i}(\kappa\xi+\lambda y)}\right]. \quad (4)$$

The problem is decoupled with respect to different slanted horizontal wave numbers of the perturbation, which are often also expressed in terms of the corresponding wavelength $\lambda_\parallel$ and azimuth angle α between the perturbation wave vector and the ξ-axis via $(\kappa, \lambda) = (2\pi/\lambda_\parallel)(\cos\alpha, \sin\alpha)$. The monochromatic character of the perturbations is in interesting agreement with the ripple structure often seen in conjunction with GWs in the mesospheric OH airglow (Hecht et al., 1997, 2000; Hecht, 2004; Taylor et al., 1997).

3. Inertia–gravity waves

For IGW packets the linear instability has been examined in various investigations (Fritts and Yuan, 1989; Yuan and Fritts, 1989; Dunkerton, 1997; Kwasniok and Schmitz, 2003), and a study for monochromatic IGWs has been done by Yau et al. (2004). At statically unstable wave amplitudes, rapidly growing leading NMs are found, with a direction of propagation in the slanted horizontal with respect to the IGW which changes from transverse to parallel as the gravity wave inclination angle gets more and more vertical. At statically and dynamically stable amplitudes NM growth is, even in the inviscid-nondiffusive limit, at most rather weak, unless the IGW inclination angle is extremely steep. An open question here was, however, the potential relevance of SVs for the stability of an IGW. Also had DNS of a breaking IGW not been done yet. The study coming nearest to this is the one by Lelong and Dunkerton (1998a,b). These authors have simulated IGW breaking in a large-eddy simulation (LES) without explicit treatment of the turbulent scales. With the intention of reducing the horizontal scale of the IGW they have also used a ratio f/N which exceeds typical values for the mesosphere by about an order of magnitude.

3.1. Linear theory

To begin with a statically and dynamically stable IGW, Fig. 4 shows the factor by which either the leading NM or the leading SV grows within an optimization time $\tau = 5$ min (Achatz, 2005). The IGW has a wavelength $\Lambda = 2\pi/K = 6$ km, an inclination angle $\Theta = 89.5°$, and amplitude $a = 0.87$, the ambient Brunt–Vaisala frequency is $N = 2 \times 10^{-2}\,\mathrm{s}^{-1}$ (so that $\tau = 5$ min roughly corresponds to one Brunt–Vaisala period), the f-plane is centered at latitude 70°N, so that the smallest Richardson number in the wave is $Ri = 0.28$. Since the IGW has a nearly vertical phase propagation, the classic instability thresholds hold approximately, and there are no growing NMs. Whatever weak NM instability might exist in the inviscid-nondiffusive limit (Yau et al., 2004) is damped by viscosity and diffusion. This does not mean, however, that there is no instability at all, since the SVs can grow by a factor larger than 7 for parallel ($\alpha = 0°$) propagation in the slanted horizontal plane. Even transverse SVs ($\alpha = 90°$) can grow by a factor larger than 5.

A better understanding of the mechanisms at work can be obtained within the framework of a shear-layer approximation of the IGW, allowing a quite extensive analytical treatment of the problem (Achatz and Schmitz, 2006a,b). For reasons of simplicity the approximations $\xi \approx x$ and $\phi \approx Kz$ are used in the remainder of this subsection, holding for steep inclination angles and simulation periods short in comparison to the IGW period. As shown in Fig. 5, the phase convention (Yau et al., 2004) is such that the location in the IGW where the total static stability minimizes is at $\phi = 3\pi/2$ (see the marker). In its neighborhood

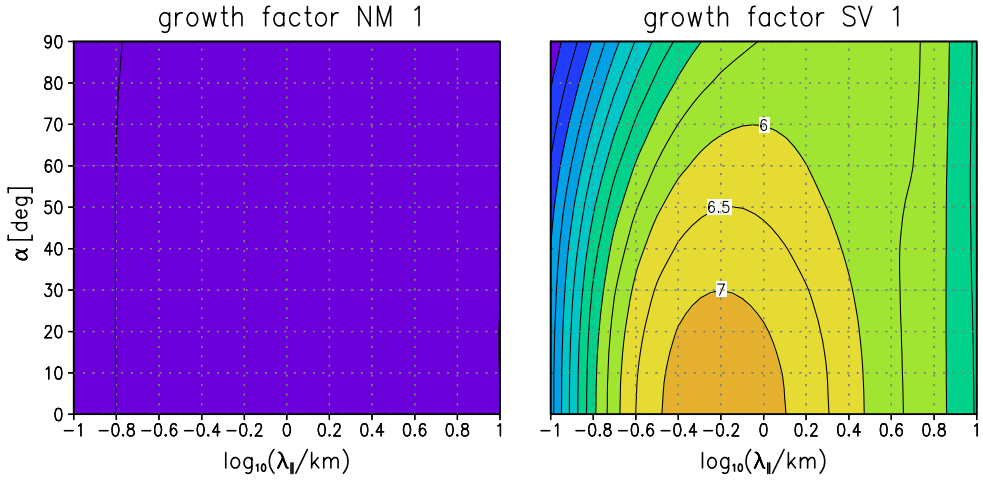

Fig. 4. In dependence on the slanted horizontal wavelength $\lambda_\parallel$ and the azimuth angle α, the factor by which the respective leading NM or leading SV of a statically and dynamically stable IGW grows within 5 min. All NM growth factors are smaller than 1. The IGW parameters are given in the main text.

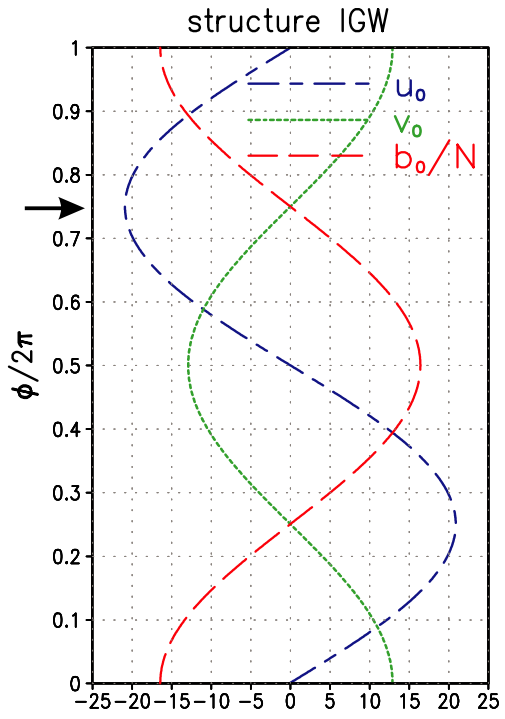

Fig. 5. Within one wavelength of a statically and dynamically stable IGW, the phase (i.e. approximately vertical) dependence of the buoyancy (normalized by the ambient Brunt–Vaisala frequency) and the horizontal flow fields in x-direction, i.e. the horizontal direction of propagation of the IGW, and in y-direction, transverse to the horizontal direction of propagation of the IGW. Units are in m/s. The location of least static stability is at $\phi = 3\pi/2$ (see the marker).

one has a locally constant flow $u_0 = U$ in x-direction, and a strongly sheared flow $v_0 \approx \beta z$ in y-direction. It turns out that this is the region where the SVs grow initially, so that a stability analysis has been done of a stratified shear layer with

$$\left(u_0,\, v_0,\, w_0,\, N^2_{\mathrm{tot}}\right) = \left[U,\, \beta z,\, 0,\, N^2(1-a)\right]. \tag{5}$$

Within this framework one finds that a parallel SV is a monochromatic wave in the x- and z-direction, and that the corresponding perturbation flow can be expressed via a stream function ψ' as $(u', w') = \mathrm{i}(-\mu, \kappa)\psi'$, where μ is the perturbation wave number in the vertical direction. In the limits $\beta^2/|N_{\mathrm{tot}}|^2 \gg 1 \gg |N_{\mathrm{tot}}|^2/N^2$ the structure of the parallel SV is then for $a < 1$ approximately

$$\begin{pmatrix}\psi' \\ v' \\ b'\end{pmatrix} \propto \mathrm{e}^{\mathrm{i}(\kappa x+\mu z-\kappa U t)-\nu k^2 t}\left[-\frac{1}{2}\mathrm{e}^{-\mathrm{i}\widehat{\omega}t}\begin{pmatrix}\Psi \\ 1 \\ B\end{pmatrix} - \frac{1}{2}\mathrm{e}^{\mathrm{i}\widehat{\omega}t}\begin{pmatrix}-\Psi \\ 1 \\ B\end{pmatrix} + \begin{pmatrix}0 \\ 1 \\ 0\end{pmatrix}\right], \tag{6}$$

where $k^2 = \kappa^2 + \mu^2$ is the squared total wavenumber of the perturbation, $\widehat{\omega} = N_{\mathrm{tot}}\kappa/k$ the intrinsic frequency of a GW in the shear layer, and $\Psi = N_{\mathrm{tot}}/(k\beta)$, and $B = N^2_{\mathrm{tot}}/\beta$. The Doppler term in the frequency of the SV results from the advection of the structure by U. The internal structure is given by the superposition of two GWs, with intrinsic frequencies $\pm\widehat{\omega}$, and a steady geostrophic mode. All components are damped by viscosity and diffusion ν (assumed to be equal). Nonetheless the energy in the structure grows: Initially the three modes interfere such that there is an exact cancellation in ψ' and v'. Since the time dependence of the three modes is different this destructive interference vanishes with progressing time, so that the SV starts growing. This is the *statically enhanced roll mechanism* which turns out to be a quite strong process.

Its energetics is also worthwhile looking at. For a general basic state depending only on the vertical one finds for the tendency of the perturbation energy

$$\frac{\mathrm{d}E}{\mathrm{d}t} = \underbrace{-\left\langle u'w'\frac{\mathrm{d}u_0}{\mathrm{d}z}\right\rangle}_{P_x} \underbrace{-\left\langle v'w'\frac{\mathrm{d}v_0}{\mathrm{d}z}\right\rangle}_{+P_y} \underbrace{-\frac{1}{N^2}\left\langle w'b'\frac{\mathrm{d}b_0}{\mathrm{d}z}\right\rangle}_{+C}. \tag{7}$$

Here viscosity and diffusion are neglected, and angle brackets indicate a global average. The two first terms in the balance are shear production terms causing E to grow due to counter-gradient fluxes of horizontal momentum in x- or y-direction. The last contribution is the convective production term which acts via counter-gradient fluxes of buoyancy. In the case of a time-dependent horizontal mean (u_0, v_0, w_0, b_0), i.e. the nonlinear case, one obtains a general budget for the exchange between the kinetic energy of the horizontal mean K_0 and that of the perturbations K, the available potential energy of the perturbations $A = b'^2/(2N^2)$ and that of the horizontal mean A_0, as indicated in Fig. 6. Convective production describes an exchange between A_0 and A, shear production an exchange between K_0 and K, and there also is the important buoyant exchange $\langle w'b'\rangle$ between A and K. Within this framework the energetics of the statically enhanced roll mechanism is shown in Fig. 7. Instead of the time derivatives of the energy the instantaneous growth rate $\Gamma = (1/2E)\mathrm{d}E/\mathrm{d}t$ is shown in its straightforward decomposition into the relevant contributing terms, such that e.g. $\Gamma_y = P_y/(2E)$ and $\Gamma_c = C/(2E)$. Fig. 7 shows a succession of two processes, another third one can only be seen by additionally looking at the decomposition of K into the components due to u', v', and w' (not shown). Initially the SV grows due to a convective exchange. This process gets especially efficient as

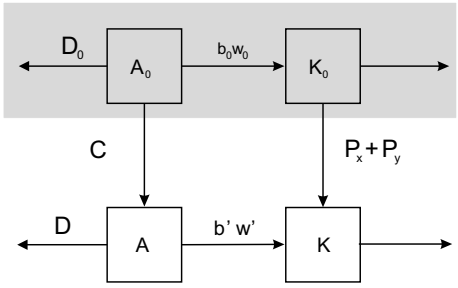

Fig. 6. Within a Boussinesq fluid on an f-plane, the budget for the energy exchange between the kinetic and the available potential energy of the slanted horizontal mean (i.e. in the linear limit the basic GW), indicated by a zero index, and the deviations from the horizontal mean. Diffusive and dissipative losses are given by D and ε.

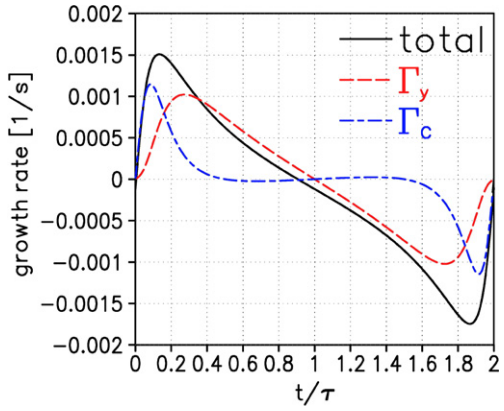

Fig. 7. The instantaneous growth rate for the parallel SV of a statically stable stratified shear layer, driven by the statically enhanced roll mechanism. Shown is the decomposition into the contributions from shear production due to counter-gradient fluxes of horizontal momentum transverse to the horizontal direction of propagation of the SV, Γ_y, and that one due to counter-gradient buoyancy fluxes, Γ_C. The optimization time is $\tau = 5$ min.

$N^2_{\text{tot}} \to 0$, so that one might speak of a statically enhanced trigger. However, this does not lead to growth in A since the energy is immediately tunnelled by the buoyant exchange into kinetic energy in w'. Provided a favorable initial perturbation in v' exists, a positive Γ_y (as seen in the figure) can lead to strong growth in the kinetic energy in v' (not shown).

An idea about the dynamics of the leading transverse SV can be obtained by considering Fig. 8. There one sees the growth-rate decomposition and the horizontally averaged density of the perturbation energy for the transverse SV of the IGW without shear-layer approximation. The early dynamics is that of a *statically enhanced Orr mechanism* which can also be discussed nicely within the shear-layer approximation (Achatz and Schmitz, 2006a,b). It is marked by an analogous static trigger as in the corresponding roll mechanism, followed by growth due to Γ_y. The latter has a different dynamics here, since the horizontal direction of propagation is parallel to the sheared velocity field in the basic state, just as in a Kelvin–Helmholtz instability. The interesting aspect about the transverse SV is that finally Γ_x takes over. This is because the SV radiates outward from the statically least stable phase region (see the energy density), so that it gets into contact with regions where $\mathrm{d}u_0/\mathrm{d}z \neq 0$. Note that the SV propagates in y-direction. We thus again have the situation under which the roll mechanism can act (vertical shear in a horizontal flow transverse to the horizontal direction of propagation of the perturbation), and indeed it starts working. Fig. 9 shows the decomposition of the perturbation energy into the four contributing terms, clearly indicating that after a rise of the energy in w' most of the energy ends up via the roll mechanism in $u'^2/2$. One can thus call the mechanism driving this SV a *statically enhanced mixed Orr and roll mechanism*.

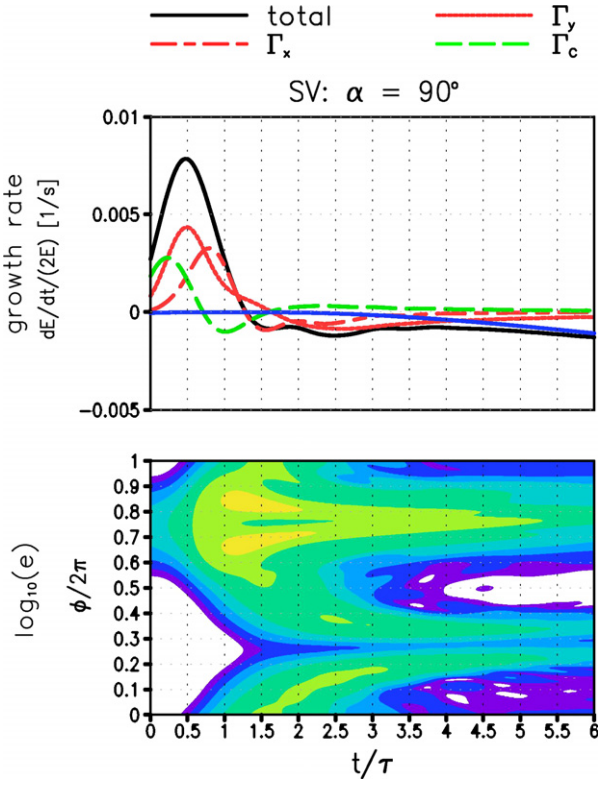

Fig. 8. For the leading transverse SV of a statically and dynamically stable IGW, the growth-rate decomposition (top panel) and the dependence of the slanted-horizontal average of the energy density $e = (1/2)(|\mathbf{v}'|^2 + b'^2/N^2)$ (bottom, linear color scale in meaningless units). The optimization time is $\tau = 5$ min. (For interpretation of the references to colour in this figure legend, the reader is referred to the web version of this article.)

3.2. Primary nonlinear dynamics

Having analyzed the linear dynamics of IGW stability one is in a much better position for understanding the results from DNS of actual IGW breaking initialized by distinctly perturbing the wave by one of the leading NMs or SVs (Achatz, 2007a). In these calculations one makes use of the fact that the spatial dependence of the initial state is two-dimensional. Rotating the two axes in the slanted horizontal plane (the ξ- and y-axis) so that the rotated ξ-axis is along the (slanted) horizontal direction of propagation of the perturbation one obtains a coordinate system within which the IGW only depends on its phase ϕ, and the perturbation on ϕ and the coordinate $x_\parallel$ along the rotated ξ-axis. The equations conserve this symmetry, unless there is a secondary perturbation with a spatial dependence transverse to the $x_\parallel$–ξ-plane. Since the velocity field is fully 3D, and the spatial dependence is not that of a conventional 2D case with dependence only on x and z, the calculations are called 2.5D. It should be stressed that the focus on the 2.5D dynamics is by intention since it highlights the primary nonlinear dynamics of the GW-breaking process, which can be used as a reference for fully 3D simulations.

Fig. 10 shows the decay of the wave amplitude after perturbing a statically unstable IGW by its leading parallel or

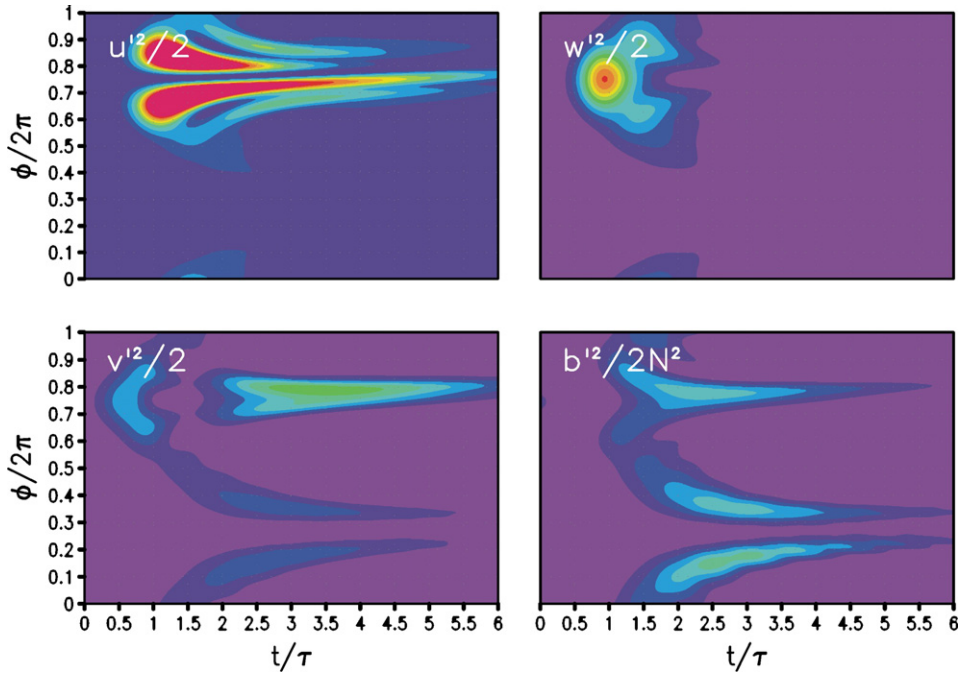

Fig. 9. For the leading transverse SV of a statically and dynamically stable IGW (as in Fig. 8), the time dependence of the slanted-horizontally averaged perturbation energy density in the three velocity fields, and in the buoyancy. The color scale is linear in meaningless units. The optimization time is $\tau = 5$ min. (For interpretation of the references to colour in this figure legend, the reader is referred to the web version of this article.)

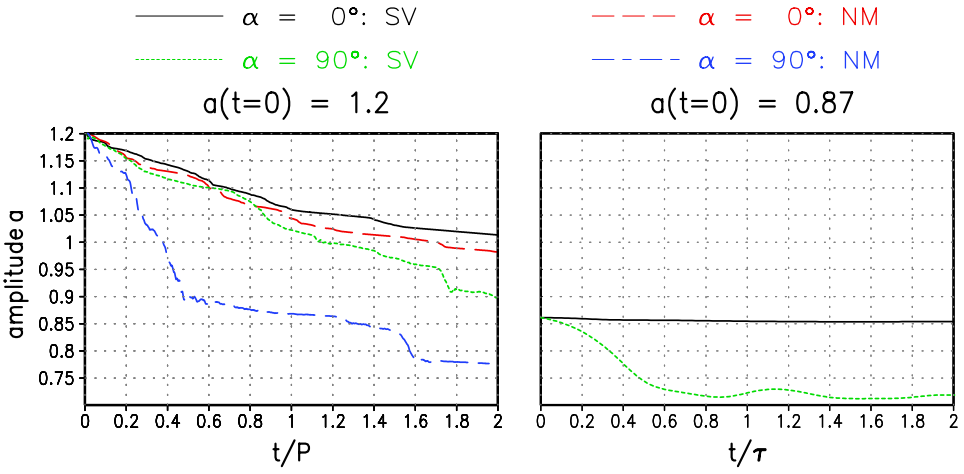

Fig. 10. The time dependence of the amplitude (with respect to the overturning threshold) of a statically unstable IGW (left panel) or a statically and dynamically stable IGW (right panel) in a DNS after having been perturbed by its leading parallel ($\alpha = 0°$) or transverse ($\alpha = 90°$) NM or SV. The wave period is $P = 7.87$ h. The optimization time is $\tau = 5$ min.

transverse NM or SV, and that of the amplitude of the statically and dynamically stable IGW analyzed above after a perturbation by its leading parallel or transverse SV.[1] Two aspects should be noted: (1) It is not only the statically unstable IGW which decays, and that to a level way below all NM instabilities, but also the statically and dynamically stable IGW. It thus is no surprise that measurements of middle atmosphere turbulence cannot always relate the observed turbulence to a static or dynamic instability (Lübken, 1997; Müllemann et al., 2003). (2) It is also interesting that in both cases the most effective perturbation is a transverse one. Indeed, the literature seems to indicate that in cases where ripples are observed simultaneously with a statically unstable IGW (Hecht et al., 1997, 2000) they have a tendency to propagate in a more or less transverse horizontal direction with respect to the IGW. The wavelength

[1] The optimization time for all SVs is $\tau = 5$ min. Although the linear theory indicates a global optimal at $\tau = 30$ min, the impact of nonlinearities prevents the corresponding SVs from undergoing their full linear growth phase, so that the SVs discussed here turn out to be the most relevant ones (Achatz, 2005; Achatz, 2007a).

of these structures is below 10 km. A simulation of ripples from a statically unstable IGW has been done by Fritts et al. (1997), where the IGW (plus an additional HGW) has been perturbed by random noise. The results here, where the leading transverse NM appears as the most effective perturbation of an IGW with $a > 1$, might give an explanation for why the occurring ripples have the observed direction of propagation. Additional support for this hypothesis might come from the wavelength of the NM (about 8 km) which is consistent with the empirical results. The weak impact of the leading transverse SV on the statically unstable IGW is mostly due to its sharp spatial confinement. It can thus only act locally on the IGW, in contrast to the NM (not shown).

The nonlinear dynamics of the leading transverse SV of the statically and dynamically stable IGW deserves a somewhat closer discussion. The major reason that this mode is more effective than the leading parallel SV is that it has larger spatial scales, and thus is less prone to be destabilized by secondary shear instabilities. It also produces turbulence of a strength as observed. Measurements suggest that the turbulent dissipation rates in the mesosphere are somewhere in the range between 1 and 10^3 mW/kg (Lübken, 1997; Müllemann et al., 2003). The DNS here shows that indeed the dissipation rate gets locally close to 10^3 mW/kg. A snapshot is given in Fig. 11. Some other interesting features can be seen there, too. There seems to be a barrier near $\phi = \pi/2$ (see the marker), which the turbulence cannot cross, and the turbulence seems to accumulate somewhere above and below the statically least stable phase range. Looking at the time dependence of the slanted horizontal average of the four contributions to the turbulent energy (Fig. 12) helps us understanding why. One sees a picture very reminiscent of Fig. 9. So indeed it is again the mixed Orr and roll mechanism which is at work here, and the accumulation of the turbulent energy at the observed maxima is due to the strong growth of $u'^2/2$ by the roll mechanism at the flanks of the statically least stable location, where the vertical gradient in the IGW wind in ξ-direction is sufficiently large. Also the barrier near $\phi = \pi/2$ can be understood based on the linear dynamics (Achatz, 2005; Achatz and Schmitz, 2006a,b; Achatz, 2007a). This is a critical line where the IGW wind in y-direction vanishes.

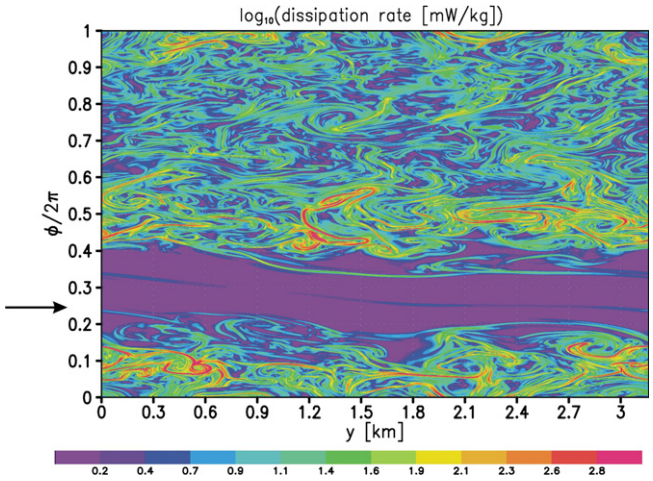

Fig. 11. The spatial dependence of the turbulent dissipation rate having developed in a DNS 15 min $= 3\tau$ after a perturbation of the statically and dynamically stable IGW by its leading transverse SV. The location $\phi = \pi/2$ is indicated by a marker.

4. High-frequency gravity waves

As discussed above, for HGWs with a non-vertical inclination angle the criteria of static and dynamic instability are not applicable. Indeed we know by now that these waves show instabilities at all amplitudes, unless damped by viscosity (Mied, 1976; Klostermeyer, 1982, 1983, 1991; Lombard and Riley, 1996a; Sonmor and Klaassen, 1997). As shown by Lombard and Riley (1996a) it is neither the wave-related shear nor the corresponding stratification which are solely responsible for the growth of linear NMs, but a mixture of the two. The orientation of the leading NM's slanted horizontal direction of propagation with respect to that of the wave depends on the wave amplitude: For statically stable HGWs the instability is predominantly 2D, i.e. the NM propagates in the same plane as the HGW. Statically unstable HGWs have leading NMs propagating transversely with respect to the wave. So far, however, the relevance of SVs for the destabilization of HGWs was still an open question. Studies of the nonlinear wave breakdown have focussed up to now on the behavior of a HGW subject to a small-amplitude random perturbation. While the first of these studies have been done at Reynolds numbers well below realistic values or using sub-grid scale models for the small-scale turbulent fluctuations (Winters and D'Asaro, 1994; Andreassen et al., 1994; Fritts et al., 1994; Isler et al., 1994; Lombard and Riley, 1996b), direct numerical simulations (DNS) with near-realistic Reynolds numbers and explicitly resolved turbulence have only recently become possible (Fritts et al., 2003, 2006). They show that the breaking of a HGW typically results in wave decay to amplitudes well below the conventional instability thresholds. The breaking of a statically and dynamically stable HGW can lead to the original wave being replaced by another secondary wave in the course of a resonant wave–wave interaction related to a parametric subharmonic instability (McComas and Bretherton, 1977; Klostermeyer, 1991; Thorpe, 1994; Vanneste, 1995). What had not been settled yet was the question whether this behavior can be tied to the HGW being perturbed by a distinct NM or SV.

4.1. Linear theory

To set the stage for the nonlinear dynamics, Fig. 13 shows for a HGW with $\Theta = 70°$ (wave period $P = 920$ s) the growth factors of the leading parallel and transverse NMs in dependence on the wave amplitude (Achatz, 2005, 2007b). At this inclination angle NMs or SVs at

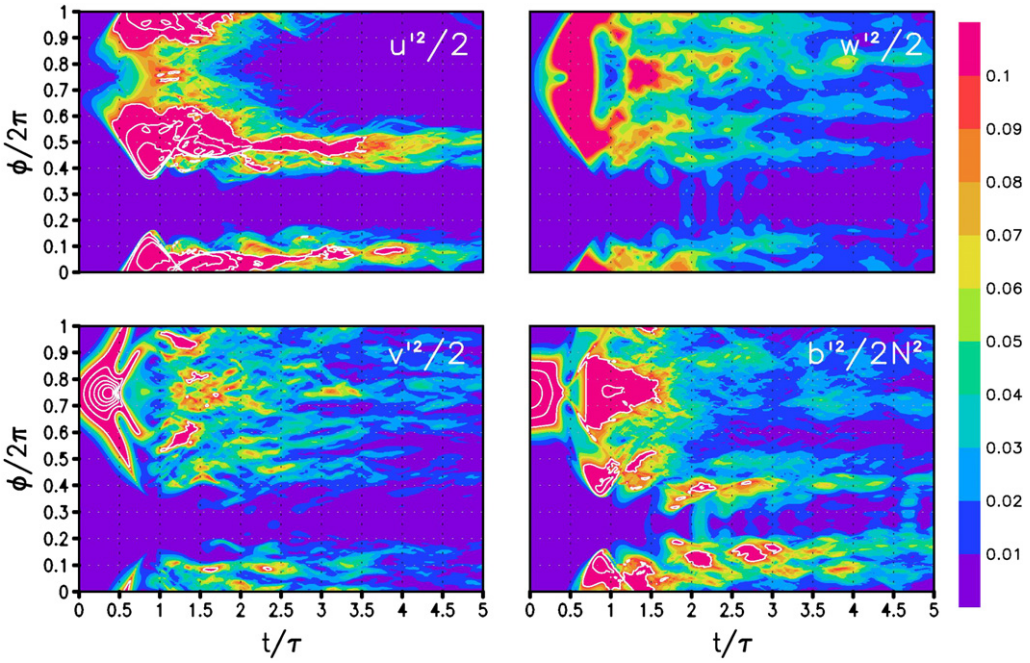

Fig. 12. Similar to Fig. 9, but now from a DNS, the time dependence of the slanted-horizontally averaged perturbation energy density in the three velocity fields, and in the buoyancy, after a perturbation of the statically and dynamically stable IGW by its leading transverse SV. All values have been normalized by the initial energy density of the IGW itself. Contours are in steps of 0.1, starting at 0.1. The optimization time is $\tau = 5$ min.

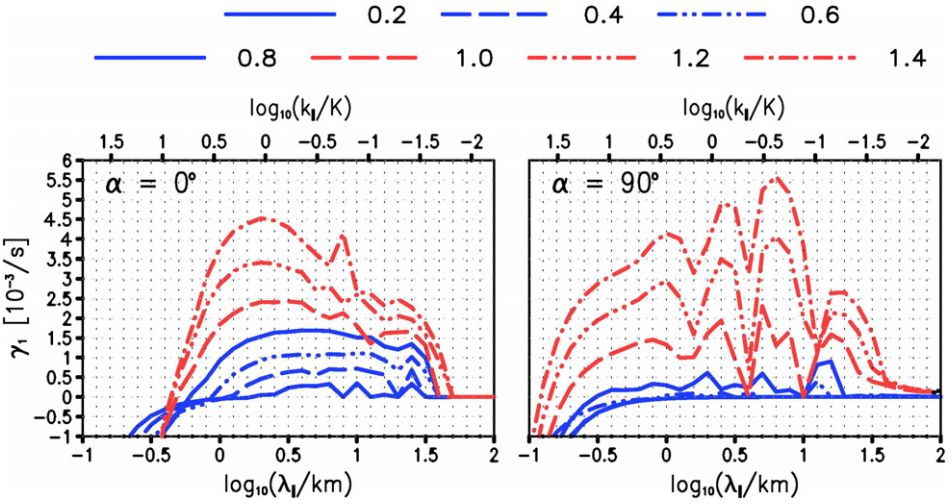

Fig. 13. For HGWs with amplitude a between 0.2 and 1.4, the growth rate of the leading parallel ($\alpha = 0°$) or transverse (90°) NM with slanted horizontal wavelength $\lambda_\parallel$ and corresponding wavenumber $k_\parallel = 2\pi/\lambda_\parallel$. Wavelength and inclination angle for all HGWs are $(\Lambda, \Theta) = (6\,\text{km}, 70°)$. $K = 2\pi/\Lambda$ is the wavenumber of the HGW.

intermediate azimuth angles are found to be mere transitions between the parallel and transverse cases. In agreement with the previous studies the statically unstable HGW is most unstable to growth of transverse NMs. As $a \to 1$ from above, the growth rates of these become, however, negligible, and the remaining growing NMs are the parallel ones. As will be shown below (Figs. 16 and 18) the reason for this is contrary to what one would expect from the amplitude with respect to the overturning threshold: At the statically unstable amplitudes it is an especially positive contribution from the shear production which causes the transverse NMs to grow more rapidly then the parallel ones. At the statically stable amplitudes it is the convective production which especially causes the parallel NMs to grow. Both of these effects are certainly due to the horizontal gradients in the basic wave. The reader should also note the secondary growth-rate peak for parallel NMs at large wavelengths. As will be seen below the corresponding NMs can be quite relevant for low-amplitude HGWs.

Once again one finds the SVs to grow over a finite time more rapidly than the corresponding NMs (Achatz, 2005).

This might not be so interesting since there is NM growth, but a relevant aspect could be the spatial distribution of the SVs. Fig. 14 shows as an example the growth-rate decomposition and slanted-horizontally averaged energy density of the leading parallel and transverse SV of the same HGW as above, with $a = 1.0$. While the NMs are rather broad structures which are spread more or less smoothly over the whole phase range of the HGW (not shown), the SV is a very localized feature. In the chosen reference frame it seems to move upward, but one should recall that this coordinate system moves downward at the phase velocity of the HGW. So actually the SV is frozen in the flow while the HGW moves over it, repeatedly exciting and damping the perturbation, again depending on the phase of the HGW which the SV is exposed to. Here the growth-rate decomposition is to be understood as above, so that e.g. $\Gamma_P = -\langle \mathbf{v}' u'_\phi \cdot K \mathrm{d}\mathbf{v}_0/\mathrm{d}\phi \rangle$ with u_ϕ being the velocity in ϕ-direction, and a zero index indicating the mean over the slanted-horizontal coordinates, i.e. in the linear limit the HGW fields.

4.2. Primary nonlinear dynamics

In their 3D DNS of a randomly perturbed HGW Fritts et al. (2003, 2006) found that the wave falls in its amplitude well below expected thresholds. An initially statically unstable HGW ends up at an amplitude $a \approx 0.3$, while an initially statically stable HGW is completely replaced by a secondary GW with steeper phase propagation. The question was whether 2.5D DNS can reproduce this behavior and thus tie it to the wave being distinctly perturbed by a dynamically meaningful NM or SV. Fig. 15 shows the HGW amplitude as it develops in such simulations after the wave has been perturbed by either its leading parallel or transverse NM (Achatz, 2007b). At the lowest chosen initial wave amplitude also the effect of a perturbation by the leading large-scale NM is shown. One sees that the results from Fritts et al. (2003, 2006) seem to be reproduced. On top of these the 2.5D DNS tell us that the breaking of a statically unstable HGW is triggered by its leading transverse NM, and that the nonlinear dynamics of an initially statically stable HGW is correctly captured in a 2.5D DNS describing the turbulent interaction between the HGW and its leading large-scale parallel NM.

The time-dependent growth rate decomposition in Fig. 16 for the eddies (i.e. the deviations from the slanted horizontal mean) in the DNS of the statically unstable HGW after a perturbation by its leading transverse NM gives some information about the dynamics of the breaking process. Although initially $a > 1$, it is not the convective production which then has the largest effect, but the shear production. This is a good example how misled we can be by expectations from traditional considerations which only take the vertical gradients into account. In the later phase damping by diffusion and dissipation take the lead which is a sign that sufficiently small-scale structures have developed via a turbulent cascade. A snapshot of the turbulent dissipation rate at the time $t = 1200\,\mathrm{s} \approx 1.3P$ of largest

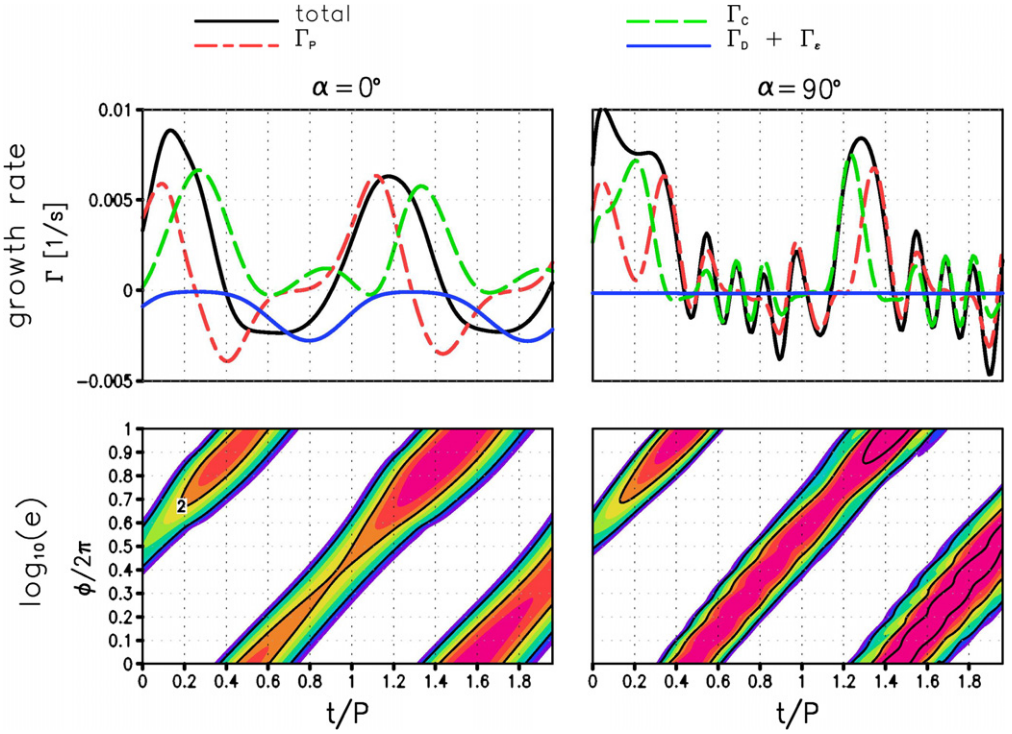

Fig. 14. Time-dependence of the amplification-rate decomposition (top row) and energy density (bottom, contours and color scale in meaningless units) from 30-min integrations of the leading parallel ($\alpha = 0$) and transverse ($\alpha = 90°$) SV (optimization time $\tau = 5$ min) for a HGW with $(\Theta, a) = (70°, 1)$. The wave period is $P = 920$ s. (For interpretation of the references to colour in this figure legend, the reader is referred to the web version of this article.)

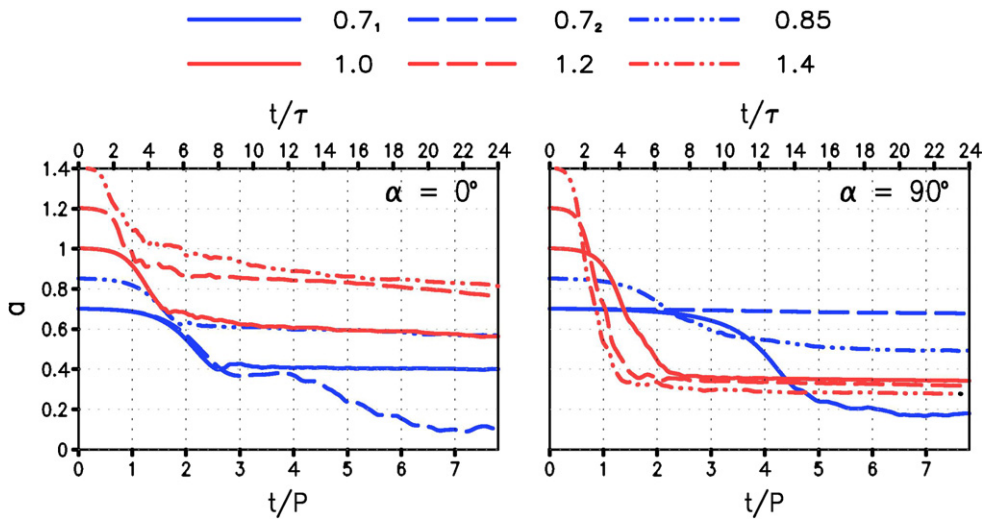

Fig. 15. From simulations of the nonlinear development of HGWs with initial amplitude a between 0.7 and 1.4 after a perturbation by the leading (and leading secondary, i.e. large-scale, for $a = 0.7$) parallel (left panel) or transverse NM (right panel), the amplitude of the basic HGW with respect to its overturning threshold. The wave period P is 920 s. For easier comparison time has also been normalized by the SV optimization time $\tau = 5$ min used below.

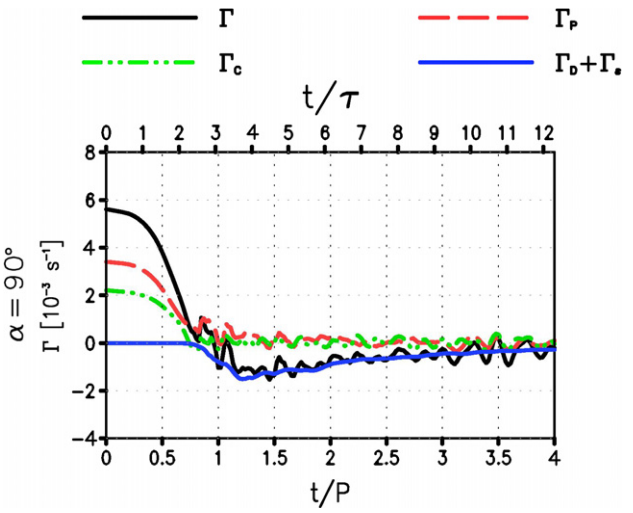

Fig. 16. From the integration of a HGW with initial $a = 1.4$, perturbed by its leading transverse NM, the decomposition of the total amplification rate Γ into its contributions from convective production Γ_C, shear production Γ_P, and viscous-diffusive damping $\Gamma_D + \Gamma_\varepsilon$. For easier comparison the time scale has been normalized both by the HGW period $P = 920$ s and the SV optimization time $\tau = 5$ min used elsewhere.

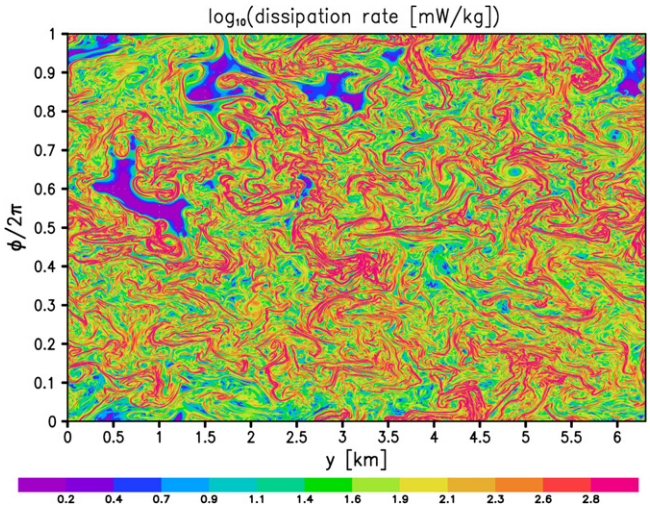

Fig. 17. From the integration of a HGW with initial $a = 1.4$, perturbed by its leading transverse NM, the spatial distribution of the turbulent dissipation rate at $t = 20$ min $\approx 1.3P$ when the viscous-diffusive damping is largest.

viscous-diffusive damping in Fig. 17 illustrates this further. One sees there also that the breaking of a statically unstable HGW produces a turbulent intensity well consistent with the upper bounds of available mesospheric measurements.

The energetics of the breaking of an initially statically stable HGW after a perturbation by the leading large-scale parallel NM is illustrated in Fig. 18. Here, too, the initial linear dynamics is contrary to more conventional expectations. Although the wave is statically stable, the NM grows, and the leading contribution to the initial NM growth is from the convective terms. As is shown by Achatz (2007b), the 2.5D DNS results in the HGW being replaced by a secondary wave with steeper phase propagation, as in Fritts et al. (2006). Important aspects of this are due to wave–wave interactions, but the process is again rather turbulent. Fig. 19 shows the spatial distribution of the turbulent dissipation rate after five HGW periods, when the viscous-diffusive damping is largest. The turbulence is weaker than in the case of the breaking of a statically unstable HGW, but the generated values are still consistent with the measurements. On average one obtains dissipation rates of several mW/kg. On the whole the most turbulent phase is more smoothly spread over the phase range of the HGW than in the other case.

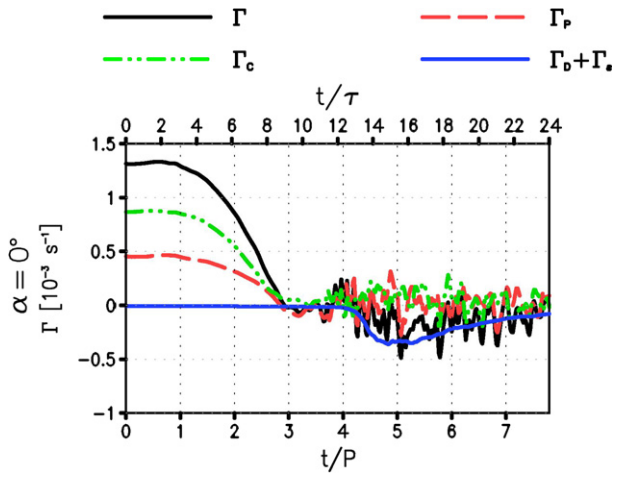

Fig. 18. From the integration of a HGW with initial $a = 0.7$, perturbed by its leading large-scale parallel NM, the decomposition of the total amplification rate Γ into its contributions from convective production Γ_C, shear production Γ_P, and viscous-diffusive damping $\Gamma_D + \Gamma_\varepsilon$. For easier comparison the time scale has been normalized both by the HGW period $P = 920$ s and the SV optimization time $\tau = 5$ min used elsewhere.

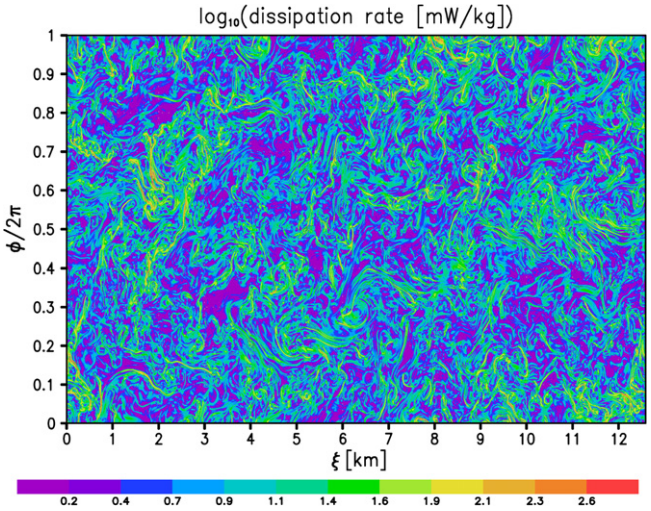

Fig. 19. From the integration of a HGW with initial $a = 0.7$, perturbed by its leading large-scale parallel NM, the spatial distribution of the turbulent dissipation rate at $t = 5P = 4600$ s when viscous-diffusive damping is largest.

A final remark shall also be made about the possible role of SVs in mesospheric HGW breaking. The 2.5D DNS in Achatz (2007b) show no major impact of the SVs on the wave. This is found to be mainly due to the extreme vertical confinement of these structures so that they can modify the HGW only very locally. An interesting aspect is, however, that for this very reason SVs might be an interesting candidate for the explanation of the sharp turbulent layers found sometimes in the measurements (Müllemann et al., 2003). Indeed, the turbulent dissipation rate from a perturbation of a statically unstable HGW ($a = 1.4$) by its leading transverse SV (for $\tau = 5$ min) after the optimization time, shown in Fig. 20, is confined to a layer of about 2–3 km width.

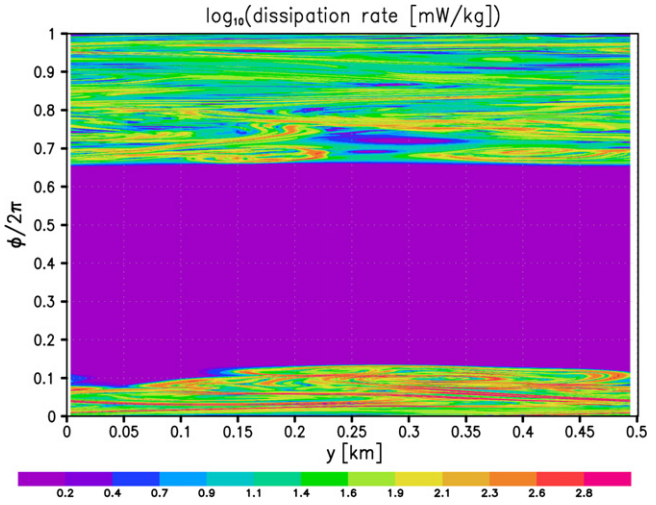

Fig. 20. From the integration of a HGW with initial $a = 1.4$, perturbed by its leading transverse SV, the spatial distribution of the turbulent dissipation rate after one optimization period $\tau = 5$ min. The initial amplitude of the SV is such that its local peak energy density is identical to the energy density of the HGW.

5. Summary and discussion

With the intent to improve our present understanding of GW breaking in the atmosphere and ocean recent work summarized in this paper has first delved into the corresponding linear theory, and then moved on to extend its results to the nonlinear domain. Perhaps a case to be made on that basis is how helpful it can be to take this kind of systematic approach. It turned out to be decisive for finally being able to also interpret many features of the complex nonlinear simulations.

An extension of the linear theory has been achieved by the application of generalized stability theory (Farrell and Ioannou, 1996a,b) to GWs. It is found that quite strongly growing SVs exist even in cases where, as for statically and dynamically stable IGWs, no NM instabilities are found. With regard to the interpretation of turbulence measurements in a statically and dynamically stable environment (e.g. Müllemann et al., 2003) this enlarges the range of possibilities we have. So far the only way to understand such measurements on the basis of GW breaking has been to assume the existence of a HGW with sufficiently strong horizontal gradients. The 2.5D DNS show that the breaking of statically and dynamically stable IGWs initialized by SV perturbations can lead to turbulent dissipation rates consistent with available observations. It also leads to an IGW decay far below presently employed instability thresholds which present parameterization schemes do not yet have on the list. Certainly this is conditioned on the GW being exposed to perturbations of sufficient initial strength, but a scenario where this could be the case is that of the GW moving into a region with fossil turbulence from a previous breaking event.

Conceptually the linear theory turns out to be quite enlightening. Especially attractive is the possibility to

understand important aspects of the core dynamics of SVs for IGWs on the basis of an analytic theory for a stratified shear layer with reduced static stability. The fundamental processes at work are found to be the statically enhanced Orr and roll mechanism, each of them interacting in a specific way with the shear in the wave, but substantially aided in doing so by a vertical convective transport due to the reduced static stability. Based on the analytic theory important aspects of the non-simplified optimal-growth process can be understood, be it with regard to the dependence on the optimization time (not discussed here), the detailed mechanisms, or the NM interference (between two GWs and a geostrophic mode) at the heart of the whole.

Special emphasis should be given to the importance of the roll mechanism. It turns out that the spatial distribution of the turbulence in a decaying IGW is to a large part controlled by the action of this mechanism in the elliptically polarized flow field of the IGW. A specific feature resulting from this is that a perturbation preferentially grows in turbulent energy in the horizontal flow component transverse to its direction of propagation, but parallel to the sheared wind, perhaps offering the possibility of an experimental test.

Similarly, the decay of HGWs can also be understood better on the basis of the linear theory. In agreement with corresponding predictions transverse NMs turn out to be most important for the breaking of a statically unstable HGW, and parallel NMs take this role for statically stable HGWs. Due to its strong local confinement the SV feedback on the HGW is rather weak. As also visible in the linear theory, however, the SVs take the character of thin turbulent layers frozen in the flow, with dissipation rates which can, depending on the initial perturbation level, be sufficiently strong so that SVs might contribute to the explanation of the conspicuous layering of turbulence often seen in the middle atmosphere (e.g. Müllemann et al., 2003; Strelnikov et al., 2003).

A special case shall also be made for the type of DNS reported here. Based on the linear results it is 2.5D, i.e. the GW is perturbed specifically by either a NM or a SV, so that the spatial dependence is restricted to the direction of phase propagation of the GW and the slanted horizontal direction of propagation of the perturbation. The simulated velocity field, however, is fully 3D, and one is not limited to the simulation of the impact of perturbations propagating in the same plane as the GW. True, one might expect that 3D secondary instabilities will eventually modify the results from these DNS, but the latter provide a reference frame within which fully 3D simulations can be discussed more easily. As an example, several findings from the 3D DNS of breaking HGWs by Fritts et al. (2003, 2006) are reproduced, with the difference that we can now say which perturbation they can be attributed to. This is not to say that 3D simulations are not necessary, on the contrary they are indispensable for providing a complete picture, but 2.5D DNS seem to be an additional helpful tool.

An important message from the theory to observers and experimentalists is that the concepts of static and dynamic stability are not appropriate criteria for the exclusion of the possibility of GW breaking and corresponding onset of turbulence. On the contrary (1) it is found that statically and dynamically stable IGWs can be destabilized by SVs, and (2) statically and dynamically stable HGWs have long been known to be unstable to NMs. In the latter case it is the horizontal gradients in the GWs which are indispensable for a complete picture. So, as attractive as it might be to have a criterion which only relies on vertical gradients, there seems to be a growing need to gather as much information as possible on the horizontal dependence of the ambient large scale (i.e. mesoscale) fields so as to be really able to understand where observed turbulence comes from. An important step here would be simultaneous measurements of all GW parameters (horizontal and vertical wavelength, and the amplitude) together with the turbulence. Linear stability analyses as described here could provide first clues as to where the turbulence onset comes from, to be later accompanied by DNS of the nonlinear behavior.

What have we learned so far which might be relevant for parameterizations? Again perhaps the most important message is that wave breaking sets in earlier, and that GWs deposit much more of their momentum than typically assumed nowadays. Partly this was already clear from the previous literature on the linear theory of NM instabilities of HGWs and corresponding 3D DNS, but it is supplemented by the additional option of IGW decay due to the impact of nonmodal perturbations, and as a whole none of these findings has yet found its way into a parameterization scheme. Unfortunately, a major problem remaining is the question as to whether it is possible to understand and predict the final amplitude of the GW, and whether and which other GWs it produces in the course of the process. Next to the GW properties, this also seems to be sensitively dependent on the specific initial perturbations and their strength. Much work remains to be done here.

Nonetheless, it is the author's belief that the systematic approach taken here, from the linear theory to the 2.5D DNS, was already able to shed more light on the GW stability problem. It seems worthwhile to continue following this path. An important aspect to be studied systematically are secondary instabilities indeed, to all expectations leading to a full three-dimensionalization of the turbulent fields (Klaassen and Peltier, 1985; Winters and D'Asaro, 1994; Andreassen et al., 1994; Fritts et al., 1994). Another task that deserves attention in the future is the certainly difficult one of the parameterization of turbulence in breaking GWs. The available DNS data might be used for testing and improving corresponding sub-grid scale schemes so that eventually LES models (e.g. Germano et al., 1991; Lilly, 1992; Ferziger, 1996; Meneveau et al., 1996) might be available which could be applied with confidence to the problem. This might then open the option of studies of whole GW spectra developing both in space and time,

a scenario which is presumably of great relevance. Once this is possible, but probably only then, we might gather new hope for more trustworthy GW parameterization schemes than the ones we have at present.

References

Achatz, U. On the role of optimal perturbations in the instability of monochromatic gravity waves. Phys. Fluids 17 (094107), 1–27, 2005.

Achatz, U. The primary nonlinear dynamics of modal and nonmodal perturbations of monochromatic inertia–gravity waves. J. Atmos. Sci. 64, 74–95, 2007a.

Achatz, U. Modal and nonmodal perturbations of monochromatic high-frequency gravity waves: Primary nonlinear dynamics. J. Atmos. Sci., in press, 2007b.

Achatz, U., Schmitz, G. Shear and static instability of inertia–gravity wave packets: short-term modal and nonmodal growth. J. Atmos. Sci. 63, 397–413, 2006a.

Achatz, U., Schmitz, G. Optimal growth in inertia–gravity wave packets: energetics, long-term development, and three-dimensional structure. J. Atmos. Sci. 63, 414–434, 2006b.

Alexander, M.J., Dunkerton, T.J. A spectral parameterization of mean-flow forcing due to breaking gravity waves. J. Atmos. Sci. 56, 4167–4182, 1999.

Andreassen, Ø., Wasberg, C.E., Fritts, D.C., Isler, J.R. Gravity wave breaking in two and three dimensions. 1. Model description and comparison of two-dimensional evolutions. J. Geophys. Res. 99, 8095–8108, 1994.

Boberg, L., Brosa, U. Onset of turbulence in a pipe. Z. Naturforschung 43A, 697–726, 1988.

Dunkerton, T.J. Shear instability of internal inertia–gravity waves. J. Atmos. Sci. 54, 1628–1641, 1997.

Farrell, B.F. Optimal excitation of neutral rossby waves. J. Atmos. Sci. 45, 163–172, 1988a.

Farrell, B.F. Optimal excitation of perturbations in viscous shear flow. Phys. Fluids 31, 2093–2102, 1988b.

Farrell, B.F., Ioannou, P.J. Optimal excitation of three-dimensional perturbations in viscous constant shear flow. Phys. Fluids A 5, 1390–1400, 1993a.

Farrell, B.F., Ioannou, P.J. Transient development of perturbations in stratified shear flow. J. Atmos. Sci. 50, 2201–2214, 1993b.

Farrell, B.F., Ioannou, P.J. Generalized stability theory. Part I: Autonomous operators. J. Atmos. Sci. 53, 2025–2040, 1996a.

Farrell, B.F., Ioannou, P.J. Generalized stability theory. Part II: Nonautonomous operators. J. Atmos. Sci. 53, 2041–2053, 1996b.

Ferziger, J.H. Large eddy simulation, in: Gatski, T.B., Hussaini, M.Y., Lumley, J.L. (Eds.), Simulation and Modeling of Turbulent Flows. Oxford University Press, pp. 109–154, 1996.

Fritts, D.C., Alexander, M.J. Gravity wave dynamics and effects in the middle atmosphere. Rev. Geophys. 41 (1), 1003, doi:10.1029/2001RG000106, 2003.

Fritts, D.C., Yuan, L. Stability analysis of inertio-gravity wave structure in the middle atmosphere. J. Atmos. Sci. 46, 1738–1745, 1989.

Fritts, D.C., Isler, J.R., Andreassen, Ø. Gravity wave breaking in two and three dimensions. 2. Three-dimensional evolution and instability structure. J. Geophys. Res. 99, 8109–8124, 1994.

Fritts, D.C., Isler, J.R., Hecht, J.H., Walterscheid, R.L., Andreassen, Ø. Wave breaking signatures in sodium densities and OH nightglow. 2. Simulation of wave and instability structures. J. Geophys. Res. 102, 6669–6684, 1997.

Fritts, D.C., Bizon, C., Werne, J.A., Meyer, C.K. Layering accompanying turbulence generation due to shear instability and gravity-wave breaking. J. Geophys. Res. 108, 8452, doi:10.1029/2002JD002406, 2003.

Fritts, D.C., Vadas, S.L., Wan, K., Werne, J.A. Mean and variable forcing of the middle atmosphere by gravity waves. J. Atmos. Sol.-Terr. Phys. 68, 247–265, 2006.

Garcia, R.R., Solomon, S. The effect of breaking gravity waves on the dynamics and chemical composition of the mesosphere and lower thermosphere. J. Geophys. Res. 90, 3850–3868, 1985.

Germano, M., Piomelli, U., Moin, P., Cabot, W.H. A dynamic subgrid-scale eddy viscosity model. Phys. Fluids A 3, 1760–1765, 1991.

Hecht, J.H. Instability layers and airglow imaging. Rev. Geophys. 42, RG1001, doi:10.1029/2003RG000131, 2004.

Hecht, J.H., Walterscheid, R.L., Fritts, D.C., Isler, J.R., Senft, D.C., Gardner, C.S., Franke, J.S. Wave breaking signatures in OH airglow and sodium densities and temperatures. 1. Airglow imaging, Na lidar, and MF radar observations. J. Geophys. Res. 102, 6655–6668, 1997.

Hecht, J.H., Fricke-Begemann, C., Walterscheid, R.L., Höffner, J. Observations of the breakdown of an atmospheric gravity wave near the cold summer mesopause at 54N. Geophys. Res. Lett. 27, 879–882, 2000.

Hines, C.O. Internal atmospheric gravity waves at ionospheric heights. Can. J. Phys. 38, 1441–1481, 1960.

Hines, C.O. Doppler spread parameterization of gravity-wave momentum deposition in the middle atmosphere. Part 1. Basic formulation. J. Atmos. Sol. Terr. Phys. 59, 371–386, 1997a.

Hines, C.O. Doppler spread parameterization of gravity–wave momentum deposition in the middle atmosphere. Part 2. Broad spectra and quasi monochromatic spectra, and implementation. J. Atmos. Sol. Terr. Phys. 59, 387–400, 1997b.

Holton, J.R. The role of gravity wave induced drag and diffusion in the momentum budget of the mesosphere. J. Atmos. Sci. 39, 791–799, 1982.

Holton, J.R. The influence of gravity wave breaking on the general circulation of the middle atmosphere. J. Atmos. Sci. 40, 2497–2507, 1983.

Houghton, J.T. The stratosphere and mesosphere. Q. J. R. Meteorol. Soc. 104, 1–29, 1978.

Howard, L.N. Note on a paper of John W. Miles. J. Fluid Mech. 10, 509–512, 1961.

Isler, J.R., Fritts, D.C., Andreassen, Ø., Wasberg, C.E. Gravity wave breaking in two and three dimensions. 3. Vortex breakdown and transition to isotropy. J. Geophys. Res. 99, 8125–8138, 1994.

Klaassen, G.P., Peltier, W.R. The onset of turbulence in finite-amplitude Kelvin–Helmholtz billows. J. Fluid Mech. 155, 1–35, 1985.

Klostermeyer, J. On parametric instabilities of finite-amplitude internal gravity waves. J. Fluid Mech. 119, 367–377, 1982.

Klostermeyer, J. Parametric instabilities of internal gravity waves in Boussinesq fluids with large Reynolds numbers. Geophys. Astrophys. Fluid Dyn. 26, 85–105, 1983.

Klostermeyer, J. Two- and three-dimensional parametric instabilities in finite amplitude internal gravity waves. Geophys. Astrophys. Fluid Dyn. 61, 1–25, 1991.

Kwasniok, F., Schmitz, G. Radiating instabilities of internal inertio-gravity waves. J. Atmos. Sci. 60, 1257–1269, 2003.

Lelong, M.P., Dunkerton, T.J. Inertia–gravity wave breaking in three dimensions. Part I: Convectively stable waves. J. Atmos. Sci. 55, 2473–2488, 1998a.

Lelong, M.P., Dunkerton, T.J. Inertia–gravity wave breaking in three dimensions. Part II: Convectively unstable waves. J. Atmos. Sci. 55, 2489–2501, 1998b.

Lilly, D.K. A proposed modification of the Germano subgrid-scale closure method. Proc. IBM Scientific Computing Symp. Environ. Sci. 4, 633–635, 1992.

Lindzen, R.S. Turbulence and stress owing to gravity wave and tidal breakdown. J. Geophys. Res. 86, 9707–9714, 1981.

Lombard, P.N., Riley, J.R. Instability and breakdown of internal gravity waves. I. Linear stability analysis. Phys. Fluids 8, 3271–3287, 1996a.

Lombard, P.N., Riley, J.R. On the breakdown into turbulence of propagating internal waves. Dyn. Atmos. Oceans 23, 345–355, 1996b.

Lübken, F.-J. Seasonal variation of turbulent energy dissipation rates at high latitudes as determined by in situ measurements of neutral density fluctuations. J. Geophys. Res. 102, 13441–13456, 1997.

McComas, C.H., Bretherton, F.P. Resonant interaction of oceanic internal waves. J. Geophys. Res. 82, 1397–1412, 1977.

Medvedev, A.S., Klaassen, G.P. Vertical evolution of gravity wave spectra and the parameterization of associated gravity wave drag. J. Geophys. Res. 100, 25841–25854, 1995.

Meneveau, C., Lund, T.S., Cabot, W.H. A Lagrangian dynamic subgrid-scale model of turbulence. J. Fluid Mech. 319, 353–385, 1996.

Mied, R.P. The occurrence of parametric instabilities in finite amplitude internal gravity waves. J. Fluid Mech. 78, 763–784, 1976.

Miles, J.W. On the stability of heterogeneous shear flows. J. Fluid Mech. 10, 496–508, 1961.

Müllemann, A., Rapp, M., Lübken, F.-J. Morphology of turbulence in the polar summer mesopause region during the MIDAS/SOLSTICE campaign 2001. Adv. Space Res. 31, 2069–2074, 2003.

Müller, P., Holloway, G., Henyey, F., Pomphrey, N. Nonlinear interactions among internal gravity waves. Rev. Geophys. 24, 493–536, 1986.

Sonmor, L.J., Klaassen, G.P. Toward a unified theory of gravity wave stability. J. Atmos. Sci. 54, 2655–2680, 1997.

Staquet, C., Sommeria, J. Internal gravity waves: from instabilities to turbulence. Annu. Rev. Fluid Mech. 34, 559–593, 2002.

Strelnikov, B., Rapp, M., Lübken, F.-J. A new technique for the analysis of neutral air density fluctuations measured in situ in the middle atmosphere. Geophys. Res. Lett. 30, 2052, doi:10.1029/2003GL018271, 2003.

Taylor, M.J., Pendleton Jr., W.R., Clark, S., Takahashi, H., Gobbi, D., Goldberg, R.A. Image measurements of short-period gravity waves at equatorial latitudes. J. Geophys. Res. 102, 26283–26299, 1997.

Thorpe, S. Observations of parametric instability and breaking waves in an oscillating tilted tube. J. Fluid Mech. 261, 33–45, 1994.

Trefethen, L.N., Trefethen, A.E., Reddy, S.C., Driscoll, T.A. Hydrodynamic stability without eigenvalues. Science 261, 578–584, 1993.

Vanneste, J. The instability of internal gravity waves to localized disturbances. Ann. Geophys. 13, 196–210, 1995.

Warner, C.D., McIntyre, M.E. An ultrasimple spectral parameterization for nonorographic gravity waves. J. Atmos. Sci. 58, 1837–1857, 2001.

Winters, K.B., D'Asaro, E.A. Three-dimensional wave instability near a critical level. J. Fluid Mech. 272, 255–284, 1994.

Wunsch, C., Ferrari, R. Vertical mixing, energy, and the general circulation of the oceans. Ann. Rev. Fluid Mech. 36, 281–314, 2004.

Yau, K.-H., Klaassen, G.P., Sonmor, L.J. Principal instabilities of large amplitude inertio-gravity waves. Phys. Fluids 16, 936–951, 2004.

Yuan, L., Fritts, D.C. Influence of a mean shear on the dynamical instability of an inertio-gravity wave. J. Atmos. Sci. 46, 2562–2568, 1989.